Journal of Biomechanics 95 (2019) 109302

Contents lists available at ScienceDirect

Journal of Biomechanics

journal homepage: www.elsevier.com/locate/jbiomech
www.JBiomech.com

Modelling the dynamic margins of stability for use in evaluations of balance following a support-surface perturbation

Keaton A. Inkol, Lori Ann Vallis *

Human Health and Nutritional Sciences, University of Guelph, Canada

ARTICLE INFO

Article history:
Accepted 31 July 2019

Keywords:
Balance
Support-surface perturbation
Center of mass
Dynamic stability
Optimization

ABSTRACT

The dynamic margin of stability provides a method that captures the center of mass (CoM) state (position-velocity) in relation to the base of support (BoS). However, the model upon which this concept was derived does not consider how the inertial characteristics of forced support-surface perturbations would influence balance control. Within the current article, the inverted pendulum model was restructured to account for fixed, piecewise accelerations of the BoS. From this logic, two variations of the adjusted margin of stability, each maintaining a similar definition of extrapolated CoM, are proposed; one ignoring horizontal ground contact and inertial forces applied to the BoS, the other incorporating these forces. Unique within the proposed models is the time-variant BoS boundaries that depend on the perturbation applied. Verification of the solution for each model is provided, along with a comparison of obtained values to previous methods of defining CoM position-velocity stability metrics using a computational model and optimal control. For the simpler model variation (*ignoring forces*), we also assessed how CoM position and perturbation parameter selection over/underestimate the predicted maximal permissible velocity. The results of these analyses suggest that factors which increase the acceleration impulse decrease the difference between the two models; the opposite was observed for factors increasing displacements between the CoM and BoS boundary. Lastly, use of the proposed adjusted margin of stability within an experimental data set highlights the ability of our model to predict instability (stepping strategies; negative margin of stability) relative to the use of the extrapolated CoM alone.

1. Introduction

Models used to evaluate the control of balance have evolved significantly over the past two decades. Classic models have characterized upright balance as an inverted pendulum, which requires the position of the whole-body center of mass (CoM) to remain within the boundaries of the base of support (BoS) to prevent a fall (Geursen et al., 1976; Winter, 1995). This condition is based on the proportional relation between the ankle joint moment, generated via dorsi-/plantarflexor activity, and center of pressure (CoP) displacement, which is constrained to remain within the BoS.

To more accurately express the dynamic nature of balance control, Pai and Patton (1997) proposed that CoM velocity must also be considered within the system. Via numerical methods, these authors established the region within CoM position-velocity space (feasible stability region; FSR) for which the inverted pendulum remains upright provided, (*i*) the initial conditions are within said region's boundaries and (*ii*) the control strategy is optimal. In response to Pai and Patton (1997), Hof et al. (2005) disseminated an analytical solution to the CoM position-velocity problem using the linear pendulum model from Winter (1995). They proposed that the control of balance could be assessed using the extrapolated CoM (xCoM; CoM position adjusted using velocity). Frequently within the literature, xCoM *position* within the BoS is the outcome measure of choice, i.e., the dynamic margin of stability (MoS). Its simplicity in execution provides researchers a means of evaluating the effects of various factors on dynamic balance: aging (Bierbaum et al., 2013; McCrum et al., 2016), dual-tasking (Bohm et al., 2012; Inkol et al., 2018a; Worden and Vallis, 2016), and during activities of daily living (de Kam et al., 2016; Marone et al., 2014).

One prominent assumption within the Hof et al. (2005) solution is that the inverted pendulum operates with one degree-of-freedom (d.o.f) and a static BoS. For researchers studying balance control, this constraint may not be ideal; under controlled conditions, such as the characterization of balance responses following a support-surface (platform) perturbation (Hurt et al., 2011; Mansouri et al., 2016; Rajachandrakumar et al., 2018; Welch and

* Corresponding author at: Human Health and Nutritional Sciences, University of Guelph, 50 Stone Road East, Guelph, Ontario N1G 2W1, Canada.
E-mail address: lvallis@uoguelph.ca (L.A. Vallis).

https://doi.org/10.1016/j.jbiomech.2019.07.046
0021-9290/

Ting, 2009), this assumption is violated. Previous work suggests that, for these perturbation experiments, the instant of time within the acceleration waveform should influence the maximal velocity the system can terminate; the result of the *acceleration* and *deceleration* phases of the platform in succession (Pai et al., 2000). Unfortunately, these researchers provided no numerical corrections for varying perturbation characteristics and used a nonlinear model, for which there may be no closed-form solution to approximate the stable boundaries.

A key component of platform perturbations is the transfer of some destabilizing tangential force via the foot-ground contact. The Winter (1995), Winter et al. (1998) model, upon which the xCoM concept is based, ignored these forces as they are of low magnitude during quiet standing (i.e. < 1 N). For cases in which the BoS is accelerating and/or rapid termination of large horizontal CoM velocities is required, this assumption cannot be true (Horak et al., 1989; Horak and Nashner, 1986). It is unclear at this time the degree to which the inclusion of ground contact forces may influence the boundaries of stability in original balance control models.

The current analyses set out to address this gap in the literature by establishing a mathematical rationale for adjusting the MoS calculations proposed by Hof et al. (2005). An inverted pendulum model designed to evaluate dynamic balance control for these paradigms was developed with two variations. One variation maintained the same foot-ground assumptions of the Winter (1995) model; the other incorporated tangential forces applied to the BoS. Our proposed analytical solutions will place emphasis on perturbations of piecewise, square-wave form (see work of Maki and colleagues; 1996). Consistency of each solution with the literature was confirmed via direct optimal control to generate the respective model variation's FSR (Pai et al., 2000; Yang et al., 2009). In this case, the FSR was multivariate; the maximal permissible initial CoM velocity was dependent on both initial CoM position and time (with respect to the perturbation waveform).

The proposed solutions were further used to demonstrate how CoM position and the factors related to perturbation parameter selection (pulse duration, acceleration magnitude, and interpulse delay) influence the difference between the proposed model variations' upper FSR boundaries (FSR error). These factors were selected as they commonly vary between experiments (Maki et al., 1996; Trivedi et al., 2010; Welch and Ting, 2009). Because additional foot-ground forces in the second model variation could limit the feasible ankle torques for balance regulation, we predicted that an increasing monotonic relationship would exist between FSR error and the following: factors that impact acceleration impulse (pulse duration and magnitude), in addition to CoM position, as larger displacements permit larger FSR velocities but require substantial ground reaction forces to halt. Lastly, both proposed MoS functions were validated against experimental kinematic data of balance recovery strategies evoked by platform perturbations. Nomenclature used throughout is summarized in Table 1.

Table 1
Nomenclature for abbreviations used throughout the text.

CoM	Whole-body centre of mass
CoP	Centre of pressure
BoS	Base of support
MoS	Dynamic margin of stability
FSR	Feasible stability region
ODE	Ordinary differential equation
$\theta, \dot{\theta}, \ddot{\theta}$	Angular position of whole-body CoM (equivalent to ankle joint angle) and its time derivative
x_c, $\dot{x}_c$, $\ddot{x}_c$	Anteroposterior position of the whole-body CoM and its time derivatives
$\ddot{x}_b$	Acceleration of the BoS (assuming it is welded to the platform)
m	Body mass (excluding feet)
m_f	Combined mass of feet
ℓ	Pendulum length, for sagittal plane ℓ is 1.24 times leg length (Hof et al., 2005)
h	Vertical height of the ankle
g	Gravitational acceleration (scalar, 9.81 m/s^2); gravity vector $\vec{g} = (-g)\hat{\mathbf{j}}$
τ	Ankle joint torque (i.e. dorsi/plantarflexor moment)
μ	Fixed position of the CoP within BoS-fixed frame
G_x	Horizontal ground reaction force
p_1, p_2	Acceleration and deceleration constants (magnitude and direction of platform acceleration with associated pulse)
A_0	Perturbation onset (start of acceleration pulse)
A_f	Termination of acceleration pulse
D_0, D_f	Onset and termination of deceleration pulse
Sh	Inverted pendulum model with moving BoS that incorporates horizontal ground reaction forces, i.e. foot ground shear forces
NSh	Inverted pendulum model with moving BoS that ignores horizontal ground reaction forces
ω	Pendulum eigenfrequency, $\omega = \sqrt{g/\ell}$
ω_1	Coefficient applied to $(x_c - \mu)$ term in pendulum ODE arising from inclusion of foot-ground shear forces
c_2	Coefficient applied to $\ddot{x}_b$ in pendulum ODE from inclusion of foot-ground shear forces
γ	Extrapolated CoM (equation varies between NSh and Sh models)
$\mu'_+(t)$, $\mu'_-(t)$	Maximum and minimum time-variant BoS boundaries (anterior and posterior in the sagittal example provided)
μ_{max}, μ_{min}	Maximum and minimum static BoS boundaries
ξ_+, ξ_-	Forward and backward MoS in the sagittal plane example
ξ_{min}	The minimum MoS

2. Model

2.1. Linear inverted pendulum model

The model proposed by Winter (1995) is a one d.o.f inverted pendulum with a point mass m fixed at length ℓ from the axis of rotation (ankle joint; Fig. 1). Assuming angles of sway θ with respect to the vertical are small, the approximations

$$d\theta \approx \frac{dx_c}{\ell}, \quad \sin(\theta) \approx \theta, \quad \cos(\theta) \approx 1 \tag{1}$$

yield the dynamical system

$$m\ell\ddot{x}_c = mgx_c(t) + \tau \approx (x_c(t) - \mu)mg \tag{2}$$

given

$$\tau = -\mu mg \tag{3}$$

The linear second-order differential equation (ODE) in (2) describes human balance control in terms of horizontal CoM accelerations $\ddot{x}_c$. Moving forward in this derivation, consider the positive x direction to be synonymous with the direction of fall induced by perturbation. To avoid falling, ankle torque τ must counteract the toppling moment produced by gravity g (acting at CoM). Assuming the ground reaction force vertical component is constant and the horizontal component can be ignored, τ can be related to CoP position μ, with respect to the ankle, by (3). The optimal solution for termination of a forward CoM momentum via maximal effort requires μ to be a fixed constant existing at the forward-most BoS boundary.

2.2. Addition of support-surface perturbations

To address the behaviour of the inverted pendulum with a controlled platform perturbation, an additional d.o.f is added. One perturbation commonly used to evoke postural responses within an experimental setting is a square-wave acceleration waveform (Inkol et al., 2018a; Maki et al., 1996; Pai et al., 2000). These particular time-varying horizontal accelerations of the BoS $\ddot{x}_b(t)$ can be shown as

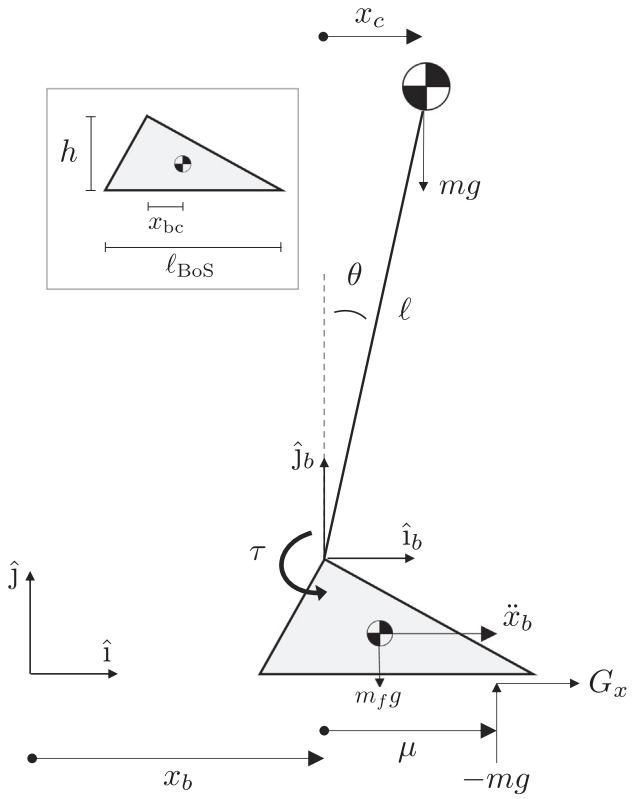

Fig. 1. Inverted pendulum model with the addition of a support-surface perturbation via base of support accelerations $\ddot{x}_b$. Note that center of mass position x_c is written within the reference frame attached to the ankle joint $(\hat{i}_b, \hat{j}_b)$.

$$\ddot{x}_b(t) = \begin{cases} p_1 & A_0 \le t < A_f \\ p_2 & D_0 \le t < D_f \\ 0 & \text{else} \end{cases} \tag{4}$$

The piecewise function (4) consists of an acceleration pulse (p_1 in $[A_0, A_f)$), quiet phase (no accelerations in $[A_f, D_0)$) and deceleration pulse (p_2 in $[D_0, D_f)$) following which, the platform comes to rest. For example, a backward support-surface translation used to evoke a forward fall (Fig. 1) would require $p_1 < 0$ and $p_2 > 0$.

The addition of (4) as an inertial force within the linear system (2) returns the revised ODE for CoM control

$$\ddot{x}_c = \omega^2(x_c(t) - \mu) - \ddot{x}_b(t) \tag{5}$$

Note here, we introduce the pendulum's eigenfrequency $\omega = \sqrt{g/\ell}$ as originally proposed by Hof et al. (2005) and used throughout his subsequent work (Hof, 2008; Hof and Curtze, 2016). A more detailed derivation of the model dynamics can be reviewed in the web based Supplementary Data file.

2.3. Solution to initial value problem

The solution for $x_c(t)$ can be derived as an initial value problem, which requires provision of an initial CoM position $x_c(0) = x_0$ and velocity $\dot{x}_c(0) = \dot{x}_0$. Using the Laplace transform of (5) allows us to convert this ODE into a simpler algebraic problem (Appendix A1). Referring to the original solution to (2) from Hof et al. (2005) as $o(t)$, *their Eq.* (3), the component of $x_c(t)$ that determines behaviour of the now 2 d.o.f pendulum in response to a support-surface perturbation is thus

$$x_c(t) = o(t) + \frac{1}{\omega^2}\{p_1[\phi_\beta(t, A_f) - \phi_\alpha(t, A_0)] + p_2[\phi_\alpha(t, D_f) - \phi_\alpha(t, D_0)]\} \tag{6}$$

where

$$\begin{aligned} \phi_\alpha(t, T) &= (\cosh[\omega(t-T)] - 1)H(t-T) \\ \phi_\beta(t, T) &= 2\sinh^2[\tfrac{1}{2}\omega(t-T)]H(t-T) \end{aligned} \tag{7}$$

contains the Heaviside function

$$H(t) = \begin{cases} 0 & t < 0 \\ 1 & t \ge 0 \end{cases} \tag{8}$$

to induce controlled changes in BoS acceleration that fit a square-wave step function.

2.4. Adjusted margin of stability

The condition that dictates whether a *forward* $\dot{x}_0$ can be terminated/reversed given some x_0 can be stated as satisfying the condition,

$$\lim_{t\to\infty} x_c(t) = -\infty \tag{9}$$

The factors that determine the limit of (6) can be established using the exponential properties of the hyperbolic functions. Thus, similar to Hof et al. (2005), the case of (9) is true if and only if the following relationship exists at $t = 0$:

$$\mu + \frac{1}{\omega^2}\{p_1(e^{-\omega A_0} - e^{-\omega A_f}) + p_2(e^{-\omega D_0} - e^{-\omega D_f})\} \ge x_0 + \frac{\dot{x}_0}{\omega} \tag{10}$$

Therefore, we can tailor the xCoM derived anterior MoS (ξ_+) at an instant t, for the case of a forward fall induced by a postural perturbation (4), as

$$\xi_+ = \mu'_+(t) - \gamma \tag{11}$$

where $+$ indicates the forward direction in our example. The planar xCoM γ is expressed as

$$\gamma = x_c + \frac{\dot{x}_c}{\omega} \tag{12}$$

while the anterior BoS boundary $\mu'_+(t)$ is now time-variant,

$$\mu'_+(t) = \mu_{\max} + \frac{1}{\omega^2}\{p_1[\psi(t, A_0) - \psi(t, A_f)] + p_2[\psi(t, D_0) - \psi(t, D_f)]\} \tag{13}$$

where

$$\psi(t, T) = e^{-\omega(T-t)H(T-t)} \tag{14}$$

For evaluation of stability in the opposing direction via μ'_-, the maximal anterior BoS boundary $\mu_{\max}$ would be switched to the minimum boundary (see Section 3.3).

2.5. Adjusted margin of stability with shear foot-ground contact

The $\mu'_+(t)$ from (13) relies on the Eq. (3) relation between τ and μ (Winter et al., 1998). If we consider the linearized horizontal ground reaction force G_x and inertial force due to BoS accelerations, τ can instead be modelled as

$$\tau(t) = -\mu mg - hm\ddot{x}_c(t) - \frac{1}{2}h(2m + m_f)\ddot{x}_b(t) \tag{15}$$

which varies in time with CoM/BoS accelerations (Appendix A2). These forces will be denoted together as shear/tangential forces

moving forward. Note that h is vertical ankle height and m_f is BoS mass, i.e., combined feet mass (Fig. 1); body mass m excludes foot mass. Substituting (15) into (2) results in the modified ODE

$$\ddot{x}_c = \omega_1^2(x_c(t) - \mu) - c_2^2\ddot{x}_b(t) \tag{16}$$

where

$$\sqrt{\omega_1} = \frac{g}{\ell + h}, \quad \sqrt{c_2} = 1 + \frac{m_f h}{2m(\ell + h)} \tag{17}$$

Using (16) with the steps outlined in 2.3–2.4, results in a dynamic MoS equation that accounts for the shear forces driving CoM perturbations as,

$$\begin{aligned} &\gamma = x_c + \tfrac{\dot{x}_c}{\omega_1}, \\ &\mu'_+(t) = \mu_{\max} \\ &\quad + \left(\tfrac{c_2}{\omega_1}\right)^2 \{p_1[\psi(t, A_0) - \psi(t, A_f)] + p_2[\psi(t, D_0) - \psi(t, D_f)]\} \end{aligned} \tag{18}$$

where $\psi(t,T) = e^{-\omega_1(T-t)H(T-t)}$ now makes use of ω_1. The two model variations proposed, and their resulting MoS (11,18), will be referred to as no shear (NSh) and shear (Sh) respectively.

3. Methods

3.1. Simulation of feasible stability region

To verify the MoS from NSh and Sh ODEs (5) and (16) were consistent with the dynamic stability definitions in the literature (Pai et al., 2000), dynamic optimization was used to generate each model's FSR. Simulations were performed using torque-driven dynamics (2). Model parameters (e.g. height, segment masses) were adopted from Pai and Patton (1997). During simulations, position of the CoP was estimated from the predicted τ using either (3) or (15) depending on the model variation (Sh, NSh) being assessed. Perturbation parameters were selected such that $\int_0^{D_f}(\ddot{x}_b)dt = 0$; values for the three conditions simulated are listed in Table 2. Briefly, the backward perturbations were akin to Maki et al. (1996) with variations in the accleration and deceleration pulses; these were of equal duration ($A_f - A_0 = D_f - D_0$) and equal/opposite magnitude ($p_2 = -p_1$). No delay existed between pulses (interpulse delay $= D_0 - A_f = 0$).

Direct collocation was used to solve the optimal control problem

$$\{x_c(t), \dot{x}_c(t), \tau(t)\} = \arg\max\left(\frac{\dot{x}_c(t_0)}{\omega}\right) \tag{19}$$

subject to the system dynamics (2) and the constraints outlined in Table 2. The desired CoM position/velocity ($x_c(t), \dot{x}_c(t)$) and $\tau(t)$ trajectories maximized the *initial* forward CoM velocity (at t_0), resolved in the BoS-fixed frame, that could be terminated within the BoS. Trajectories were discretized into 10–25 ms intervals over a total period of 2–3 sec. Eq. (19) was solved for all combinations of normalized initial CoM positions $[0, 0.25, 0.50, \ldots, 1.50]$, i.e., $(\mu_{\max} - x_c)/\ell_{\text{BoS}}$ (ℓ_{BoS} = BoS length), and initial times $[0, 0.1D_f, 0.2D_f, \ldots, D_f]$ (perturbation onset at $t = 0$). The returned velocities constructed the upper boundary of the discrete 3D FSR; each FSR corresponded to a set combination of acceleration magnitude and pulse duration. Optimization was achieved using a gradient-based solver (*fmincon*) within the MATLAB (version 9.4) Optimization Toolbox (The MathWorks, Inc, Natick, MA).

3.2. Approximating error between two feasible stability regions

A descriptive approach, involving calculation of an FSR error matrix $[\varepsilon]$, was used to quantitatively assess the element-wise error between two discrete FSR. Matrix $[\varepsilon]$ was calculated as

$$[\varepsilon] = [F_1(t, x_c) - F_2(t, x_c)] \tag{20}$$

Note that for the case of numerically derived FSR, t and x_c were initial conditions corresponding to each simulation. The elements of $[\varepsilon]$ for any comparison were subsequently used to construct boxplots which could be examined to assess the differences between two underlying methods.

Numerical validation of the Sh and NSh solutions involved comparisons, via (20), of the FSR returned via optimal control with the evaluated analytical FSR for each model. These FSR error were examined for the three conditions introduced in Section 3.1 (Table 3). To establish the effects of our factors of interest (pulse duration, acceleration magnitude, interpulse delay, CoM position; values outlined in Table 3) on the permitted maximal velocity returned by NSh and Sh models, FSR error sensitivity was also assessed. Conditions in Table 3 were defined by variations in one factor while the others were held constant; for each condition, the FSR for both models was calculated across 100 points spaced evenly between $t = 0$ (perturbation onset) to $t = D_f$. Not shown in Table 3, *normalized* CoM position was maintained at $x_c = 0.5$ when examining just the effects of the perturbation parameters.

3.3. Experimental data

Data from our previous published work (Inkol et al., 2018b) was used to assess the efficacy of the proposed Sh and NSh $\mu'(t)$

Table 2
Constraint functions imposed on the parameterized state and control trajectories within the optimal control (dynamic optimization) routine used to solve for the feasible stability regions of the linear inverted pendulum with support-surface perturbations.

Constraint	Algebraic equation	Notes
System Dynamics		$\underline{x}_t = \{x_c(t), \dot{x}_c(t)\}^T$
Linearized pendulum	$\underline{x}_{t+1} - \underline{x}_t - \Delta t(d\underline{x}_t/dt) = 0, \forall t \geq 0$	Δt = 10 – 25 ms
CoM initial conditions		
Position	$\xi_{\text{tgt}} - \ell_{\text{BoS}}^{-1}(\ell_{\text{a2t}} - x_c(t_0)) = 0$	ξ_{tgt} was adjusted per simulation
CoM terminal conditions		
Position	$\min\{\mu_{\max} - x_c(t_f), x_c(t_f) - \mu_{\min}\} > 0$	$\mu_{\max} = \ell_{\text{a2t}}$
Velocity	$\dot{x}_c(t_f) = 0$	$\mu_{\min} = -\ell_{\text{a2h}}$
Acceleration	$\ddot{x}_c(t_f) = 0$	t_f = 2.00 – 3.00 s
Ground Contact		
Center of pressure	$\min\{\mu_{\max} - \mu(t), \mu(t) - \mu_{\min}\} > 0, \forall t \geq 0$	$\mu(t)$, see Eqs. (3,15)
Vertical ground reaction	$10^{-3}[m\ddot{y}_c(t) + g(m + m_f)] > 0, \forall t \geq 0$	* $\ddot{y}_c$ calculated using nonlinear dynamics

Unique Terms: tgt – target; a2t – ankle-to-toe distance; a2h – ankle-to-heel distance.

Table 3
Perturbation parameters used to populate Eq. (4) within the following procedures: the three simulation conditions; examination of the differences between the feasible stability region generated by the NSh and Sh models; the experimental protocol in which the proposed MoS is validated. For the Sh vs. NSh comparisons, the range of values assigned to the parameter to be tested are shown in brackets; the interval(s) tested within this range is the δ in the first column.

Condition	p_1(m/s^2)	p_2(m/s^2)	A_0(s)	A_f(s)	D_0(s)	D_f(s)
Simulated						
i	−1.00	1.00	0	0.20	0.20	0.40
ii	−1.00	1.00	0	0.30	0.60	0.60
iii	−2.00	2.00	0	0.30	0.60	0.60
Sh vs. NSh						
Pulse duration (δ = 0.20)	−1.00	1.00	0	[0.00,..,0.60]	[0.00,..,0.60]	[0.00,..,1.20]†
Accel. Magnitude (δ=±1)	-[1.00,..,3.00]	[1.00,..,3.00]	0	0.30	0.30	0.60
Interpulse delay (δ = 0.20)	−1.00	1.00	0	0.30	[0.30,..,0.90]	[0.60,..,1.20]
CoM position*	−1.00	1.00	0	0.30	0.30	0.60
Experimental						
Small forward	0.73	−0.73	2.00	2.30	2.60	2.60
Small backward	−1.00	1.00	2.00	2.30	2.60	2.60
Large forward	2.20	−2.20	2.00	2.30	2.60	2.60
Large backward	−3.00	3.00	2.00	2.30	2.60	2.60

* Initial CoM position is varied parameter; normalized positions used (w.r.t to BoS length) are [0.00, 0.50, 1.00, 1.50].
† Set is [0.00, 0.40, 0.80, 1.20].

functions. These data were from three healthy young adults (2 males; 21–23 years; mean ± SD height = 175 ± 20 cm, weight = 66 ± 13 kg); each participant provided informed written consent to take part in the protocol approved by the University of Guelph Research Ethics Board. In brief, the experimental protocol required participants to maintain upright balance following a given support-surface perturbation; fixed-support strategies were encouraged through verbal instruction. Perturbations were of eight potential combinations adopted from Maki et al. (1996) (parameters shown in Table 3). For the current study, we focused on one trial per small/large magnitude support-surface translation (backward and forward).

Position and velocity of the CoM were estimated using low-pass filtered (cut-off: 6 Hz) 3D kinematic data (100 Hz; Optitrack, NaturalPoint, Corvallis, OR, USA) and the weighted segmental average method (Winter et al., 1998). Platform position was subtracted from marker position data to resolve the MoS within the platform/BoS-fixed frame. Anteroposterior BoS boundaries were defined using markers located on the first toe (μ_{max}) and the heel (μ_{min}). These boundaries were then used to calculate the sagittal minimum MoS using the original Hof et al. (2005) formulation and proposed NSh/Sh models (adjusted MoS) as

$$\xi_{min} = \min\{\mu'_{+} - \gamma, \gamma - \mu'_{-}\} \quad (21)$$

For small magnitude perturbations (i.e. no stepping), ξ_{min} was evaluated at the instance of peak perturbation velocity; this event coincides with the maximal xCoM excursion within these trials (Inkol et al., 2018a, 2018b). For large magnitude trials, ξ_{min} was evaluated at step initiation as has been reported in previous work (Bhatt et al., 2006; Pai et al., 2000, 1998).

4. Results

Representative MoS trajectories generated using each model (NSh, Sh, and Hof et al. (2005)) for the small backward perturbation trial are displayed in Fig. 2A. Despite the participant requiring no steps, the Hof model returned negative values; in contrast the proposed Sh and NSh models yielded near identical positive MoS curves. Fig. 2B is an example of the FSR upper boundary for the NSh model for a large backward perturbation (Table 3). Fig. 2C presents the FSR error for the NSh/Sh analytical models relative to their corresponding numerical FSR across perturbation conditions. The FSR generated from our analytical solutions were near-identical to those derived via numerical methods (FSR error $\leq$ |4| mm) regardless of whether acceleration magnitude or pulse duration were altered. Table 4 highlights the ability of our proposed MoS metrics over the Hof et al. (2005) model in predicting the occurrence of stepping response following a platform perturbation (unstable, $\xi_{min} < 0$). In particular, the small magnitude perturbations (i.e. no stepping) consistently produced $\xi_{min} \geq 0$ when using NSh or Sh; ξ_{min} at step initiation following a large perturbation was always negative. Using the Hof et al. (2005) model produced negative values across all conditions.

Error associated with shear force exclusion (NSh vs. Sh) in determining FSR of the inverted pendulum model is reported in Fig. 3. With no BoS accelerations, reverting the NSh model back to Hof MoS model, FSR error was minimal across the horizon of interest $[A_0, D_f]$ (approx. 4 mm at $x_c = 0.5$). Increasing pulse duration or acceleration magnitude had the surprising effect of monotonically reducing FSR error; however, variability across the horizon increased. Altering the interpulse delay had minimal effect on the difference between the NSh and Sh. The CoM position had the largest influence on FSR error; the further the CoM was from the maximal (anterior) boundary, the larger the discrepancy between the Sh and NSh models.

5. Discussion

5.1. Perturbation dependent stability margins

The addition of platform perturbations within the linearized inverted pendulum equation of motion facilitated an expansion of the BoS definition beyond that of the feasible CoP position. In our proposed analytical model, postural responses could be modeled as dependent on the function that defines controlled platform accelerations. Combining the new BoS function $\mu'(t)$, that does (Sh; Eq. (18)) or does not (NSh; Eq. (13)) consider shear foot–ground force constraints, with the extrapolated CoM concept (Hof et al. 2005) yields an MoS specialized for perturbation-based experimental paradigms. Note that although the sagittal plane was of focus within the current derivations, the results presented may be transferred to the frontal plane as well.

The analytical solutions were supported by direct optimal control methods that solved for the NSh/Sh model FSRs. This draws parallels to the xCoM term Hof et al. (2005) provided with reference to the work by Pai and Patton (1997). The observed variance in error were likely a product of the selected optimization parameters (e.g., relaxed stopping criteria, initial guesses). Of particular

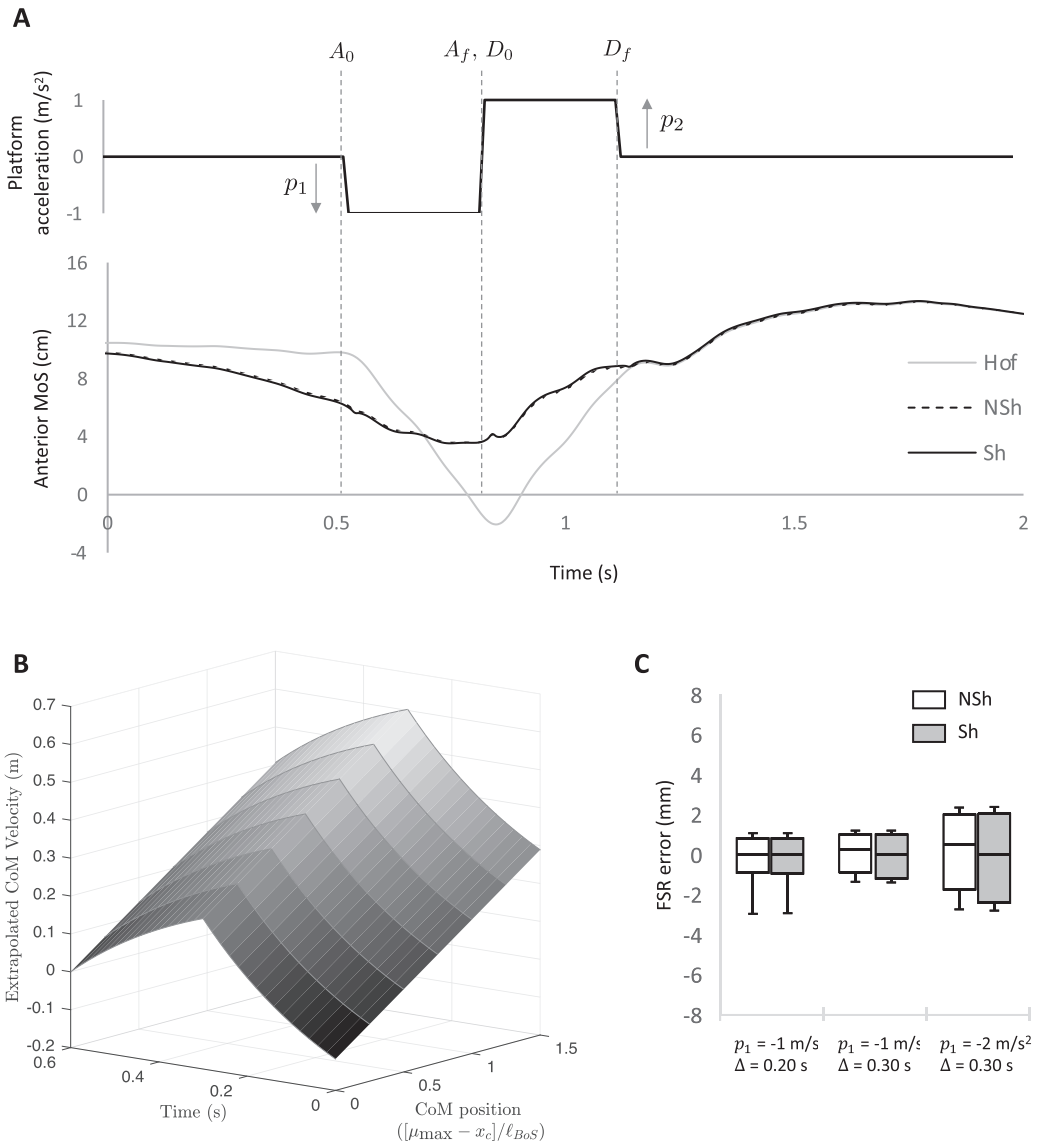

Fig. 2. A. Representative trajectories of the anterior MoS calculated using the Hof et al. (2005; grey line), NSh, and Sh models for a small backward perturbation. The perturbation parameters required for the proposed NSh and Sh models have been identified in the platform acceleration waveform above the MoS plot. Note that NSh (dotted line) and Sh (bold line) curves are effectively overlaying each other. **B.** Example of the upper boundary of the feasible stability regions (FSR) for the inverted pendulum model with support-surface perturbations ingoring horizontal ground reaction forces (i.e. NSh). Here, the upper boundary represents the maximal forward velocity (normalized to pendulum eigenfrequency ω) that can be terminated/reversed for a given CoM position (relative to anterior base of support boundary and normalized to base of support length) and instant of time within the perturbation waveform. **C.** Boxplots of the error between the analytical and simulated FSR (numerically derived via optimization) for both the NSh (*white*) and Sh (*grey*) models. (For interpretation of the references to colour in this figure legend, the reader is referred to the web version of this article.)

Table 4
Mean ± SD minimum anteroposterior margin of stability ξ_{min} calculated for each perturbation condition using the Hof et al. (2005) formulation or the measures *proposed* within the current study that either neglect (NSh) or include (Sh) horizontal ground reaction/shear forces alongside the accelerating BoS. Negative MoS corresponds to a CoM position-velocity state that cannot be corrected using an ankle strategy alone; either a step or countermovement strategy must be used. Perturbation magnitudes adopted from Maki et al. (1996) indicated as either small or large. Note that stepping response would be predicted when $\xi_{min} < 0$.

Perturbation	ξ_{min}(cm)		
	Original	NSh	Sh
Small backward	−4.8 ± 2.5	1.6 ± 2.2	1.6 ± 2.2
Large backward	−21.2 ± 2.3	−6.9 ± 5.4	−6.8 ± 5.5
Small forward	−3.7 ± 0.8	0.8 ± 0.3	0.8 ± 0.2
Large forward	−14.8 ± 3.1	−4.8 ± 3.1	−4.8 ± 3.2

importance, our proposed MoS models are quite capable of establishing a stable ($\xi_{min} > 0$)/unstable ($\xi_{min} < 0$) dichotomy in terms of balance recovery when compared to the solution obtained via calculations from Hof et al. (2005). We therefore propose that the use of either NSh or Sh MoS is best for research questions investigating how individuals maintain dynamic stability in the presence of support-surface translations, e.g., how much closer is an older adult to their stability boundary compared to a young adult following a platform perturbation.

A unique result of the current study is related to the potential for future model adaptations. Though we focused on perturbations of square-wave accelerations, it should suffice that the Laplace transform of many piecewise or continuously differentiable perturbation functions (e.g. oscillations, single sinusoid, etc.; de Kam et al., 2018; Welch and Ting, 2009) can be used in future models. The proposed function $\mu'(t)$ can thus be tailored to most

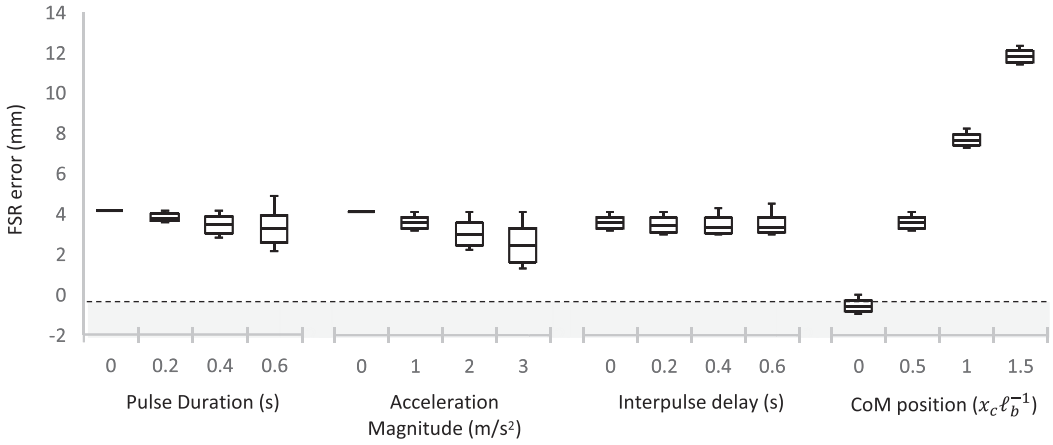

Fig. 3. Boxplots highlighting the influence of pulse duration ($= A_f - A_0 = D_f - D_0$), acceleration magnitude ($= -p_1 = p_2$), interpulse delay ($= D_0 - A_f$), and CoM position ($[\mu_{\max} - x_c]/\ell_{\text{BoS}}$) on the error between the NSh and Sh model FSR (NSh ignores foot-ground shear and $\ddot{x}_b$ inertial forces). Note that FSR error > 0 indicates an overestimation of the FSR upper boundary by the NSh model relative to Sh.

experimental perturbation conditions by solving the corresponding $x_c(t)$ via methods similar to the current study or Hof and Curtze (2016). This modeling approach is quite feasible given the availability of modern symbolic mathematical software.

5.2. Horizontal ground reaction forces and the margin of stability

Limited work has tested the assumption of negligible foot–ground shear forces for the inverted pendulum; however, there exists clear empirical evidence that these forces exceed the Winter et al. (1998) 1 N threshold (Horak et al., 1989; Horak and Nashner, 1986). Furthermore, most simulation-based studies that have solved for the FSR of varying balance models have included this force within CoP calculations (Iqbal and Pai, 2000; Pai et al., 2000; Pai and Patton, 1997).

Despite the large magnitude shear forces acting as the source of CoM perturbations, the differences between the NSh and Sh MoS/FSR were minimal. Unexpectedly, FSR error decreased when pulse duration and acceleration magnitude of the perturbation was increased. If no perturbation was present and the goal was to accelerate the CoM posteriorly, foot–ground shear forces would reduce the possible τ and the resulting FSR boundary (initial) velocity. However, comparing the solution to $x_c(t)$ from the NSh and Sh models (not shown in Results) revealed that the changes in CoM/BoS accelerations for Sh, when the CoP is treated as a fixed quantity, both limits and enables values of τ to exceed the static τ in (3). Specifically, increasing the impulse of the BoS *deceleration* allows the Sh model to generate larger compensatory torques later into the perturbation waveform when compared to NSh.

The factor that best determined whether NSh overestimated the maximal permissible velocity when ignoring shear forces was CoM position. The observed differences between NSh and Sh associated with the perturbation parameters, although expected to be larger, were quite small. Increasing these differences would demand c_2 to be of greater magnitude which inherently requires an unrealistic, large BoS (m_f, h) relative to the rest of the body (17). Hence, it may be more appropriate to select the Sh model in cases where a larger BoS is utilized, e.g., large stance width, double-support phase of gait. Regardless, the errors reported may not exceed 'functionally' defined thresholds; though, threshold placement is somewhat arbitrary in the literature as it is set primarily up to the discretion of the researcher (e.g. 2 cm, Jamkrajang et al., 2017). Therefore, we postulate that the NSh model, which requires definition of fewer parameters and has simpler coefficients, is sufficient for most cases of balance control with platform perturbations.

6. Limitations

The limitations of the inverted pendulum model have been well established by Winter et al. (1998) and Hof et al. (2005). In brief, the model is dependent on the assumption that the ankle strategy defines CoM control. Perturbations that are able to evoke counterbalancing strategies (e.g. the hip strategy; Horak and Nashner, 1986) could yield a negative MoS despite no step being evoked (Hof, 2007; Iqbal and Pai, 2000); modifications of the inverted pendulum to model countermovement/stepping strategies could address this issue (Aftab et al., 2016; Hsiao and Robinovitch, 1999). Lastly, we should not ignore the assumptions that come with model reduction, e.g., approximation of trigonometric functions. The full impact of such approximations is not clear for the case of support-surface perturbations, though it may be the case that only perturbations of certain magnitude are of concern.

Another point of interest is that the current stability margins do not intrinsically define stability in the sense of Lyapunov. The *a priori* defined CoM-CoP optimal control strategy dictates the termination of falling within a single direction; no proof of the system stability accompanies this assumption. It can then be assumed that deviations away from this 'optimal' strategy would require manipulation of said margins. Inclusion of neural delays and muscle activation dynamics that reduce the CoP to finite time excursions would be an example of such deviations and have been proposed for the xCoM concept (Hof and Curtze, 2016).

Declaration of Competing Interest

There are no conflicts of interest to report.

Acknowledgements

The authors would like to acknowledge funding provided by a NSERC Discovery Grant (awarded to LAV), Ontario Graduate Student and NSERC Master's Canada Graduate Scholarship (awarded to KAI), in addition to Canadian Foundation for Innovation and Ontario Research Fund Research Infrastructure grants for equipment. The authors would also like to extend their appreciation to Dr. John Zettel for use of laboratory equipment.

Appendix A. Solving inverted pendulum differential equation via Laplace Transform

To solve the second-order, linear differential equation

$$\ddot{x}_c = \omega^2(x_c(t) - \mu) - \ddot{x}_b(t) \tag{A.1}$$

We took the Laplace transform of each term factoring out constants when possible:

$$\frac{\mathcal{L}\{\ddot{x}_c\} + \mathcal{L}\{\ddot{x}_b(t)\}}{\omega^2} = \mathcal{L}\{x_c(t)\} - \mathcal{L}\{\mu\} \tag{A.2}$$

The s-domain transforms for our unknown function of time and its second derivative were written as

$$\mathcal{L}\{x_c(t)\} = X_c(s), \mathcal{L}\{\ddot{x}_c\} = s^2X_c(s) - \dot{x}_0 - sx_0 \tag{A.3}$$

where $\dot{x}_0 = \dot{x}_c(0)$ and $x_0 = x_c(0)$ were the initial conditions. The Laplace transform of the piecewise perturbation function (4) was simply the summation of definite integrals across subdomains within $t \geq 0$

$$\mathcal{L}\{\ddot{x}_b(t)\} = \int_{A_0}^{A_f} p_1 e^{-st}dt + \int_{D_0}^{D_f} p_2 e^{-st}dt \tag{A.4}$$

$$= \frac{p_1\left(e^{-sA_0} - e^{-sA_f}\right) + p_2\left(e^{-sD_0} - e^{-sD_f}\right)}{s} \tag{A.5}$$

Substitution of A.4 and A.6 into A.3 provides the CoM s-domain function

$$X_c(s) = \frac{s(sx_0 + \dot{x}_0) - \mu\omega^2 + p_1\left(e^{-sA_f} - e^{-sA_0}\right) + p_2\left(e^{-sD_f} - e^{-sD_0}\right)}{s(s+\omega)(s-\omega)} \tag{A.6}$$

which can then be transformed back to the time-domain and reduced to the form seen in (6).

Appendix B. Addition of foot-ground shear forces to the torque function

The relation $\tau = -\mu mg$ (3) is based on the assumption that the BoS is rotationally static (sum of applied moments about the ankle joint = 0) and that the vertical ground reaction force ($\approx mg$) is the only substantial determinant of τ. The reaction force's line of action is coincident with the CoP position μ which must remain within the BoS. Therefore, the maximal ankle torque that can be generated to correct CoM velocity is constrained by the boundary value of μ. Using this logic, we can revise (3) to consider the tangential forces acting on the BoS during support-surface translations.

From Fig. 1, assuming clockwise rotations to be positive, the sum of moments about the ankle for the static BoS provide the revised relationship.

$$\tau = -\mu mg - hG_x + \frac{h}{2}m_f\ddot{x}_b \tag{A.7}$$

which uses D'Alembert's principle to account for accelerations of the BoS $\ddot{x}_b$ as an inertial force acting on the segment CoM. Like Winter et al. (1995), gravitational toppling of the foot is ignored within this derivation. Using a Newton-Euler approach to solve for horizontal ground reaction force G_x relies on resolution of the ankle reaction forces,

$$A_x = m\left(\ddot{\vec{r}_c}\right)\hat{\imath} \tag{A.8}$$

where $\ddot{\vec{r}}_c$ is the nonlinear horizontal CoM acceleration written in terms of θ and x_b

$$A_x = m\left[\ddot{x}_b - \ell\dot{\theta}^2\sin\theta(t) + \ell\ddot{\theta}\cos\theta(t)\right]\hat{\imath} \tag{A.9}$$

Thus, applying Netwon's second law for horizontal motion of the BoS,

$$G_x - A_x = m_f(\ddot{x}_b)\hat{\imath} \tag{A.10}$$

in combination with the small-angle approximations (1) results in the linear equation

$$G_x = \left[(m + m_f)\ddot{x}_b + m\ddot{x}_c\right]\hat{\imath} \tag{A.11}$$

that may be substituted into A.7

$$\tau(t) = -\mu mg - hm\ddot{x}_c - \frac{1}{2}h(2m + m_f)\ddot{x}_b(t) \tag{A.12}$$

The permissible torque is still constrained by some maximal/minimal μ (i.e. BoS boundaries) but is now time-variant as it scales in relation to CoM/BoS accelerations.

Appendix C. Supplementary material

Supplementary data to this article can be found online at https://doi.org/10.1016/j.jbiomech.2019.07.046.

References

Aftab, Z., Robert, T., Wieber, P.-B., 2016. Balance recovery prediction with multiple strategies for standing humans e0151166 PLoS ONE 11. https://doi.org/10.1371/journal.pone.0151166.

Bhatt, T., Wening, J.D., Pai, Y.-C., 2006. Adaptive control of gait stability in reducing slip-related backward loss of balance. Exp. Brain Res. 170, 61–73.

Bierbaum, S., Peper, A., Arampatzis, A., 2013. Exercise of mechanisms of dynamic stability improves the stability state after an unexpected gait perturbation in elderly. AGE 35, 1905–1915. https://doi.org/10.1007/s11357-012-9481-z.

Bohm, S., Mersmann, F., Bierbaum, S., Dietrich, R., Arampatzis, A., 2012. Cognitive demand and predictive adaptational responses in dynamic stability control. J. Biomech. 45, 2330–2336. https://doi.org/10.1016/j.jbiomech.2012.07.009.

de Kam, D., Kamphuis, J.F., Weerdesteyn, V., Geurts, A.C.H., 2016. The effect of weight-bearing asymmetry on dynamic postural stability in healthy young individuals. Gait Posture 45, 56–61. https://doi.org/10.1016/j.gaitpost.2016.01.004.

de Kam, D., Roelofs, J.M.B., Geurts, A.C.H., Weerdesteyn, V., 2018. Body configuration at first stepping-foot contact predicts backward balance recovery capacity in people with chronic stroke e0192961 PLoS ONE 13. https://doi.org/10.1371/journal.pone.0192961.

Geursen, J.B., Altena, D., Massen, C.H., Verduin, M., 1976. A model of the standing man for the description of his dynamic behaviour. Agressologie 17 SPECNO, pp. 63–69.

Hof, A.L., 2008. The 'extrapolated center of mass' concept suggests a simple control of balance in walking. Hum. Mov. Sci. 27, 112–125. https://doi.org/10.1016/j.humov.2007.08.003.

Hof, A.L., 2007. The equations of motion for a standing human reveal three mechanisms for balance. J. Biomech. 40, 451–457.

Hof, A.L., Curtze, C., 2016. A stricter condition for standing balance after unexpected perturbations. J. Biomech. 49, 580–585. https://doi.org/10.1016/j.jbiomech.2016.01.021.

Hof, A.L., Gazendam, M.G.J., Sinke, W.E., 2005. The condition for dynamic stability. J. Biomech. 38, 1–8.

Horak, F.B., Diener, H.C., Nashner, L.M., 1989. Influence of central set on human postural responses. J. Neurophysiol. 62, 841–853. https://doi.org/10.1152/jn.1989.62.4.841.

Horak, F.B., Nashner, L.M., 1986. Central programming of postural movements: adaptation to altered support-surface configurations. J. Neurophysiol. 55, 1369–1381.

Hsiao, E.T., Robinovitch, S.N., 1999. Biomechanical influences on balance recovery by stepping. J. Biomech. 32, 1099–1106.

Hurt, C.P., Rosenblatt, N.J., Grabiner, M.D., 2011. Form of the compensatory stepping response to repeated laterally directed postural disturbances. Exp. Brain Res. 214, 557–566. https://doi.org/10.1007/s00221-011-2854-1.

Inkol, K.A., Huntley, A.H., Vallis, L.A., 2018a. Do perturbation-evoked responses result in higher reaction time costs depending on the direction and magnitude of perturbation? Exp. Brain Res. 236, 1689–1698. https://doi.org/10.1007/s00221-018-5249-8.

Inkol, K.A., Huntley, A.H., Vallis, L.A., 2018b. Modeling margin of stability with feet in place following a postural perturbation: Effect of altered anthropometric models for estimated extrapolated centre of mass. Gait Posture 62, 434–439. https://doi.org/10.1016/j.gaitpost.2018.03.050.

Iqbal, K., Pai, Y., 2000. Predicted region of stability for balance recovery: motion at the knee joint can improve termination of forward movement. J. Biomech. 33, 1619–1627.

Jamkrajang, P., Robinson, M.A., Limroongreungrat, W., Vanrenterghem, J., 2017. Can segmental model reductions quantify whole-body balance accurately during dynamic activities? Gait Posture 56, 37–41. https://doi.org/10.1016/j.gaitpost.2017.04.036.

Maki, B.E., McIlroy, W.E., Perry, S.D., 1996. Influence of lateral destabilization on compensatory stepping responses. J. Biomech. 29, 343–353.

Mansouri, M., Clark, A.E., Seth, A., Reinbolt, J.A., 2016. Rectus femoris transfer surgery affects balance recovery in children with cerebral palsy: A computer simulation study. Gait & Posture 43, 24–30. https://doi.org/10.1016/j.gaitpost.2015.08.016.

Marone, J.R., Patel, P.B., Hurt, C.P., Grabiner, M.D., 2014. Frontal plane margin of stability is increased during texting while walking. Gait Posture 40, 243–246. https://doi.org/10.1016/j.gaitpost.2014.04.188.

McCrum, C., Epro, G., Meijer, K., Zijlstra, W., Brüggemann, G.-P., Karamanidis, K., 2016. Locomotor stability and adaptation during perturbed walking across the adult female lifespan. J. Biomech. 49, 1244–1247. https://doi.org/10.1016/j.jbiomech.2016.02.051.

Pai, Y.C., Maki, B.E., Iqbal, K., McIlroy, W.E., Perry, S.D., 2000. Thresholds for step initiation induced by support-surface translation: a dynamic center-of-mass model provides much better prediction than a static model. J. Biomech. 33, 387–392.

Pai, Y.C., Patton, J., 1997. Center of mass velocity-position predictions for balance control. J. Biomech. 30, 347–354.

Pai, Y.C., Rogers, M.W., Patton, J., Cain, T.D., Hanke, T.A., 1998. Static versus dynamic predictions of protective stepping following waist-pull perturbations in young and older adults. J. Biomech. 31, 1111–1118.

Rajachandrakumar, R., Mann, J., Schinkel-Ivy, A., Mansfield, A., 2018. Exploring the relationship between stability and variability of the centre of mass and centre of pressure. Gait Posture 63, 254–259. https://doi.org/10.1016/j.gaitpost.2018.05.008.

Trivedi, H., Leonard, J.A., Ting, L.H., Stapley, P.J., 2010. Postural responses to unexpected perturbations of balance during reaching. Exp. Brain Res. 202, 485–491. https://doi.org/10.1007/s00221-009-2135-4.

Welch, T.D.J., Ting, L.H., 2009. A feedback model explains the differential scaling of human postural responses to perturbation acceleration and velocity. J. Neurophysiol. 101, 3294–3309. https://doi.org/10.1152/jn.90775.2008.

Winter, D., 1995. Human balance and posture control during standing and walking. Gait & Posture 3, 193–214. https://doi.org/10.1016/0966-6362(96)82849-9.

Winter, D.A., Patla, A.E., Prince, F., Ishac, M., Gielo-Perczak, K., 1998. Stiffness control of balance in quiet standing. J. Neurophysiol. 80, 1211–1221.

Worden, T.A., Vallis, L.A., 2016. Stability control during the performance of a simultaneous obstacle avoidance and auditory Stroop task. Exp. Brain Res. 234, 387–396. https://doi.org/10.1007/s00221-015-4461-z.

Yang, F., Espy, D., Pai, Y.-C., 2009. Feasible stability region in the frontal plane during human gait. Ann. Biomed. Eng. 37, 2606–2614. https://doi.org/10.1007/s10439-009-9798-7.